Semi-Analytical Beam Transportation Code for Heavy-Ion Radiotherapy

Taku Inaniwa[1], Takuji Furukawa[1], Naruhiro Matsufuji[1], Toshiyuki Kohno[2], Shinji Sato[1], Koji Noda[1] and Tatsuaki Kanai[1]

[1]*National Institute of Radiological Sciences: Anagawa 4-9-1, Inage-ku, Chiba 263-8555, Japan, taku@nirs.go.jp*
[2]*Department of Energy Sciences, Tokyo Institute of Technology: 4259 Nagatsuta-cho, Midori-ku, Yokohama 226-8502, Japan*

The aim of the present work is to develop a semi-analytical beam transportation code which can calculate the spatial distribution of radiation quality in a substance for heavy-ion therapy. The beam transportation code developed here is based on an elemental pencil beam model where the spatial distribution of radiation quality for an elemental beam is calculated and superposed according to the emittance ellipse of the narrow heavy-ion beam determined at the entrance of the target. In this paper, we show the calculation procedure used in the developed code in detail. Furthermore, as an example, the three-dimensional distributions of dose, LET and fluence are calculated for a mono-energetic narrow carbon beam of 290 MeV/u.

I. INTRODUCTION

The biological effectiveness of heavy ions is affected not only by the deposited energy but also by the particle species. Therefore, precise calculation for the spatial distribution of radiation quality such as dose, dose averaged LET, fluence and energy distributions for narrow heavy-ion beams is essential in the treatment planning of heavy-ion therapy where several species of fragments are generated and widely distribute in a patient's body. It is known that Monte Calro codes are time-consuming and are currently not practical for implementation into treatment planning system. Therefore, we developed a semi-analytical beam transportation code where the spatial distribution of fragment particles can be calculated. In this code, we employed an elemental pencil beam model[1] where the spatial distribution of radiation quality for an elemental beam is calculated and superposed according to the emittance ellipse of the narrow heavy-ion beam determined at the entrance of the target. In the calculation of the radiation quality for an elemental beam, we adopted a simple calculation model based on the Goldhaber model in which the spatial distribution of fragments can be represented using a single free parameter.

As an example of the calculation, we presented the three-dimensional dose distribution for the mono-energetic narrow carbon beam of 290 MeV/u.

II. CALCULATION PROCEDURE

The three dimensional beam transportation code developed here is on the basis of the elemental pencil beam model[1]. In this model, at first, an emittance ellipse in the x-x' (or y-y') phase space is determined for the narrow heavy-ion beam at the entrance of the target. Then the spatial distribution of radiation quality is calculated for each elemental pencil beam with an infinitesimally small elemental area within the ellipse. Finally, the derived distributions are superposed according to the weights given by the emittance and the twiss parameters of the narrow beam.

When the homogeneous material is chosen as the target, the radiation quality of the elemental pencil beam need to be derived only once and it can be superposed according to the weights given by the emittance and the twiss parameters of the narrow beam. For simplicity, homogeneous water was selected as the target material in this paper. However, in principle, the lateral and longitudinal heterogeneities can be taken into account in the code[2].

II.A. Elemental pencil beam

The one-dimensional semi-empirical beam transportation code 'HIBRAC' was developed to support the heavy-charged particle therapy program at the Heavy Ion Medical Accelerator in Chiba (HIMAC), National Institute of Radiological Sciences (NIRS) clinical facility[3]. In this work, the calculation method of the depth-dose, dose averaged LET, fluence and energy distribution along the beam axis is basically the same as HIBRAC. Therefore, the explanation about the derivation of these physical quantities is kept to a minimum here.

II.A.1. Transportation of primary beam

The incident charged particles lose their energies as they travel in a target and stop around their mean range. In our calculation, the target material is divided into many

thin layers in the beam direction and (a) the stopping power d*E*/ds, (b) the straggling, (c) the attenuation of the primary beam and (d) the extent of beam deflection due to multiple scattering are calculated in each layer until they come to rest by losing their energies.

(a) In the calculation of d*E*/ds, the relativistic corrections, density correction and effective charge correction at low velocities are considered while shell effect corrections are neglected.

(b) The approximation applied in the energy distribution at each depth *s*, $F(E,s)$, with a pathlength distribution $H(R,s)$:

$$H(R,s)dR = F(E,s)dE \quad (1)$$

is also used in our calculation even though it requires an additional initial energy spread in order to make up the slightly underestimated range straggling[3]. In equation (1), *R* and *E* are the range and the energy of the particle at the depth *s*.

(c) The attenuation, of the primary beam $N_0(s)$ was calculated by

$$-dN_0(s) = N_T N_0(s)\sigma[E_P(s)]ds, \quad (2)$$

where N_T denotes the number of target nuclei per unit area, and $\sigma[E_P(s)]$ is the total reaction cross section for the projectile ions of the energy E_P at a depth of s. For $\sigma[E_P(s)]$, the data parameterized by Sihver *et al* (1993)[4] was used.

(d) The extent of beam deflection due to multiple scattering can be described well using the model by Mustafa and Jackson (1981)[5], which is based on Moliere scattering theory. According to this model, the primary beam suffers the deflection characterized by the root-mean square (RMS) scattering angle θ_{RMS} when they pass through the thin target layer in which energy loss can be neglected. The total scattering angle of the beam passing through *n* layers which correspond to the depth of *s*, is given as a sum of an RMS of local scattering angle calculated for each layer:

$$\theta_{RMS}(s)^2 = \theta_{RMS(1)}{}^2 + \theta_{RMS(2)}{}^2 + \cdots\cdots + \theta_{RMS(n)}{}^2 \quad . \quad (3)$$

Then the lateral broadening of the beam $\sigma_{RMS}(s)$ due to the multiple scattering at a depth of *s* is given by

$$\sigma_{RMS}(s) = 6^{-1/2}\theta_{RMS}(s)t \, . \quad (4)$$

II.A.1. Production and transportation of secondary and tertiary fragments

Nuclear interactions will attenuate the particle fluence as described in equation (2). They will also produce fragmentations of the projectile ions and the target nuclei, and many kinds of fragments distribute in a substance. In our calculation, the productions of secondary and tertiary fragments are considered at each penetration layer, and they are treated as the incident particles after their production layers. The production of *i*th species of secondary fragment (with mass number of A_{sf_i} and atomic number of Z_{sf_i}) is given by

$$N_{sf_i}(s) = N_0(s)N_T\sigma\left[E_P(s), A_P, Z_P, A_T, Z_T, A_{sf_i}, Z_{sf_i}\right] \, . \quad (5)$$

Here, $\sigma\left[E_P(s), A_P, Z_P, A_T, Z_T, A_{sf_i}, Z_{sf_i}\right]$ denotes the partial reaction cross section for the projectile ions (with mass number of A_P and atomic number of Z_P) of the energy E_P at the depth of *s* in a target. The partial reaction cross sections parameterized by Sihver *et al* [3, 4] were used again in this calculation. The average longitudinal recoil momentum of the fragments at the reaction point in the center of mass system is proportional to the mass difference $\Delta A = A_P - A_{sf_i}$ of the projectile A_P and the fragment A_{sf_i}:

$$\left\langle P_{\parallel} \right\rangle = 8\Delta A \frac{\gamma+1}{\beta\gamma}\frac{A_{sf_i}}{A_P} \text{ [MeV/c]} \quad (6)$$

where γ is the Lorentz factor (Morrissey 1989). The momentum distribution of projectile fragments after the nuclear reaction is approximated by a Gaussian distribution (Tarasov 2004) with the standard deviation $\sigma_{\parallel}$

$$\sigma_{\parallel}{}^2 = \sigma_0{}^2 \frac{A_{sf_i}\left(A_P - A_{sf_i}\right)}{\left(A_P - 1\right)} \text{ [MeV/c]} \quad (7)$$

according to Goldhaber (1974)[6], where σ_0 is the reduced width related to the Fermi motion which is an intrinsic motion of the constituent (nucleon) of the nucleus. The value of $\sigma_0 = 52.4$ MeV/c is used throughout the present work. Since the width is considered to be isotropic in the rest frame of the fragment within the experimental uncertainty[7], the same momentum width is assumed in lateral direction as σ_{Fermi}. Therefore, we can assume that fragments suffer a lateral momentum transfer (momentum kick) at their production points, and its extent θ_{kick} can be described as

$$\theta_{kick} = \arctan\left(\sigma_{Fermi}/P_{K\parallel}\right), \quad (8)$$

where $P_{K\parallel}$ indicates the kinetic momentum of the fragment particle along the beam axis. Here, $P_{K\parallel}$ can be derived by subtracting the momentum loss (6) from the momentum of the primary particle.

The scattering angle of the *i*th species of secondary fragments at the depth of *s*, i.e., *n*th layer, can be given by

$$\theta^2_{\mathrm{RMS},i}(s)=\sum_{k=1}^{n}\left(\frac{N_{n,\mathrm{sf}_i}(k)}{N_{n,i}}\right)\left(\sum_{l=1}^{k-1}\theta^2_{\mathrm{RMS}(l,\mathrm{primary})}+\theta^2_{k,\mathrm{kick}}+\sum_{m=k}^{n}\theta^2_{\mathrm{RMS}(m,sf)}\right) \quad (9)$$

Here, the fragment is assumed to be produced at *k*th layer. Upstream of the layer *k* (from 1 to *k*-1, denoted by *l*), the lateral displacement of the beam is characterized by the multiple scattering of the primary particles. Then the produced secondary fragment particle, receiving a momentum kick $\theta_{k,\mathrm{kick}}$ in the *k*th layer, undergoes multiple scattering downstream of the reaction layer (from *k* to *n*, denoted by *m*). $N_{n,\mathrm{sf}_i}(k)/N_{n,i}$ indicates the ratio of the number of fragment *i* produced at the layer *k* and arrives at the layer *n* to the total number of the *i*th fragment arrives at the layer *n*.

When the *j*th species of tertiary fragments (with mass number of A_{tf_j} and atomic number of Z_{tf_j}) are produced by the brake-up of *i*th species of secondary fragments, the spatial distribution of them can be calculated with the similar equations as (2)-(9) by replacing the physical parameters characterizing the behaviors of the primary and the secondary fragments to those of the secondary fragments and the tertiary fragments, respectively.

In our calculation, the tertiary fragments are assumed not to be attenuated and no particles of higher order are assumed to be created.

Consequently, the scattering angle of *l*th species of fragments at the depth of *s* can be calculated

$$\theta^2_{\mathrm{RMS},l}(s)=\theta^2_{\mathrm{RMS},i=l}(s)+\theta^2_{\mathrm{RMS},j=l}(s), \quad (10)$$

where $\theta_{\mathrm{RMS},i}$ and $\theta_{\mathrm{RMS},j}$ are the RMS scattering angles of secondary and tertiary fragments. The lateral broadening of the beam, $\sigma_{\mathrm{RMS},l}(s)$, can be calculated according to equation (4).

The one-dimensional (1D) depth dose distribution and the lateral width of the elemental carbon beam of 290 MeV/u are calculated and shown in figures 1 and 2 as a function of depth in water for each particle specie with the different atomic number (Z_j =1-6).

As described at the top of this section, only the homogeneous material was chosen as the target in this paper. Therefore, the energy E_{P}, the initial energy spread of the primary beam $\sigma_{E_{\mathrm{P}}}$, species of the target and calculation step size in x, y and beam directions are chosen as input parameters for the calculation of the elemental beam.

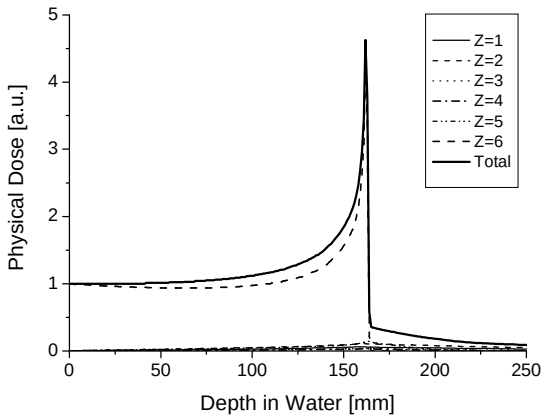

Figure 1. The 1D dose distribution of an elemental carbon beam of 290 MeV/u in water. The contribution from each specie of fragment characterized by the atomic number *Z* is shown with different line.

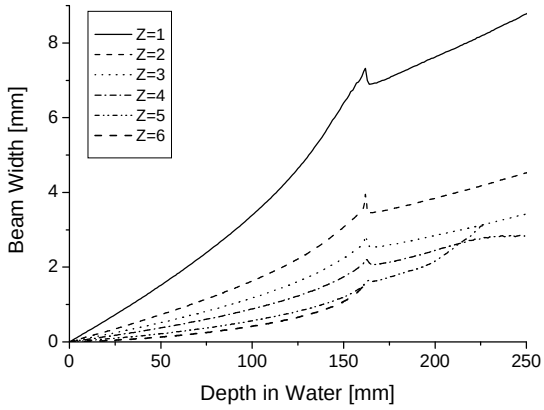

Figure 2. The lateral beam width of each specie of fragment characterized by the atomic number *Z* of an elemental carbon beam of 290 MeV/u in water.

II.B. Superposition of elemental beams

The spatial distribution of radiation quality of the narrow heavy-ion beam in a substance is affected by the emittance of the incident beam. The elemental beam with an infinitesimally small area in the phase space derived in sec II.A is superposed according to the emittance ellipse in order to describe the narrow heavy-ion beam in the substance. The emittance ellipse is defined with the emittance and the twiss parameters (ε_x, α_x, β_x) and (ε_y, α_y, β_y) in *x*-*x*' and *y*-*y*' phase space, respectively. Each ellipse is divided into small elemental areas in the phase space with (x_i, x_i' : i=1,2, …, N) or (y_i, y_i' : i=1,2, …, N), where subscript i specifies each divided area. Then the elemental beam is assigned to each of them and superposed according to the weight map given by

$$f(x,x') = \frac{1}{2\pi\varepsilon_x}\exp\left[-\frac{1}{2\varepsilon_x}\left(\gamma_x x^2 + \beta_x x'^2 + 2\alpha_x xx'\right)\right] \quad (11)$$

$$f(y,y') = \frac{1}{2\pi\varepsilon_y}\exp\left[-\frac{1}{2\varepsilon_y}\left(\gamma_y y^2 + \beta_y y'^2 + 2\alpha_y yy'\right)\right] \quad (12)$$

where $\gamma_x = \left(1+\alpha_x{}^2\right)/\beta_x$ and $\gamma_y = \left(1+\alpha_y{}^2\right)/\beta_y$.

The superposition of the elemental beams is schematically shown in figure 3. The three-dimensional (3D) distributions of dose, dose-averaged LET and fluence can be calculated for any narrow heavy-ion beams with this method.

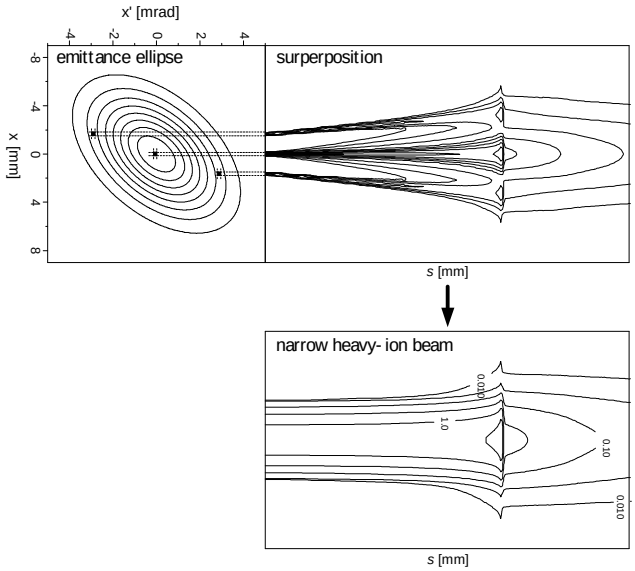

Figure 3. The superposition of elemental pencil beam with an infinitesimally small area in the phase space according to the emittance ellipse.

III. RESULTS AND DISCUSSIONS

The spatial distribution of radiation quality for the narrow heavy-ion beam, i.e., the 3D dose, the dose averaged LET, the fluence and energy distribution, can be calculated for any particle species generated in a substance with our calculation code. As an example of the calculation, the 3D dose distribution delivered by the mono-energetic carbon beam was calculated. In the calculation, a homogeneous water target was assumed to be irradiated with the narrow carbon beam of 290 MeV/u. The emittance and twiss parameters of the beam assumed at the entrance of the target were summarized in table 1. The dose distributions on the horizontal plane calculated for the particle species with different atomic numbers (Z=1-6) are shown in figures 4(a)-(f). The dose levels are identified with the different colors in each distribution, and the corresponding color scale is shown at the right hand side of the figure. Although dose levels for lighter fragments are relatively low, these particles spread widely beyond the Bragg peak. The width of the dose distribution for the particles with Z=6 gradually increase with the penetration depth and takes its maximum around the Bragg peak (around 160 mm in water), while these particles deliver no energy to the region beyond the peak.

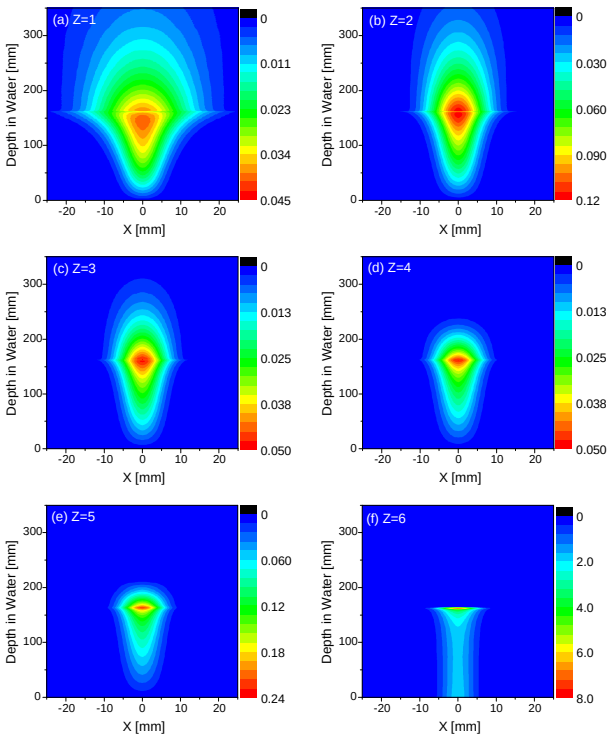

Figure 4. The dose distribution of mono-energetic 290 MeV/u ^{12}C beam on the horizontal plane for each element with the atomic number Z of (a) 1, (b) 2, (c) 3, (d) 4, (e) 5 and (f) 6.

IV. CONCLUSIONS

The radiological response of cells depends not only on the deposited energy but also on the species of incoming particles. Therefore, the precise calculation for the spatial distribution of radiation quality of a narrow heavy-ion beam is essential in the treatment planning of heavy-ion therapy where various species of fragments are produced and widely distribute in a patient's body. We developed a semi-analytical beam transportation code which could calculate the spatial distribution of projectile fragments in a substance. In this code, we employed an elemental pencil beam model where the spatial distribution of radiation quality for an elemental beam is calculated and superposed according to the emittance ellipse of the spot beam determined at the entrance of the target.

We expect that the developed code is useful to evaluate the biological effectiveness of the heavy-ion beam precisely. Furthermore, the developed calculation code can be used to derive the spatial distribution of positron emitting nuclei in a patient's body generated through fragmentation reactions of incident ions with target nuclei[8].

ACKNOWLEDGMENTS

We are very grateful to the skillful work of the HIMAC operation staff. We thank the members of the Medical Physics Research Group for their fruitful advice on our research. This work was carried out as a part of the Research Project with Heavy Ions at HIMAC.

REFERENCES

1. Schaffner B, Pedroni E and Lomax A, "Dose calculation models for proton treatment planning using a dynamic beam delivery system: an attempt to include density heterogeneity effects in the analytical dose calculation," *Phys. Med. Biol.*, **44**, 27-41 (1999).
2. Brahme A, "Development of radiation therapy optimization," *Acta Oncol*. **39** 579-595 (2000)
3. Sihver L, Schardt D and Kanai T, "Depth dose distribution of high-energy carbon, oxygen and neon beams in water," *Japan. J. Med. Phys.*, **18**, 1-22 (1998).
4. Sihver L, Tsao C H, Silberberg R, Kanai T and Barghouty A F, "Total reaction and partial cross section calculations in proton-nucleus ($Z_t \leq 26$) and nucleus-nucleus reactions (Z_p and $Z_t \leq 26$)," *Phys. Rev.* **C**, **47**, 1225-1236 (1993).
5. Mustafa A A M and Jackson D F, "Small-angle multiple scattering and spatial resolution in charged particle tomography," *Phys. Med. Biol.*, **26**, 461-472 (1981).
6. Goldhaber A S, "Statistical models of fragmentation process," *Phys. Lett.* **B 53** 306-308 (1974)
7. Golovkov M, Aleksandrov D, Chulkov L, Kraus G and Schard D, "Fragmentation of 270 A MeV carbon ions in water," *Advances in Hadrontherapy* (Amsterdam: Elsevier) pp 325-330 (1997)
8. Inaniwa T, Kohno T, Tomitani T, Urakabe E, Sato S, Kanazawa M and Kanai T, "Experimental determination of particle range and dose distribution in thick targets through fragmentation reactions of stable heavy ions," *Phys. Med. Biol.* **51** 4129-4146 (2006)